Formulation Study of Paramagnetic Fluorinated Nanoemulsions for Systemic Fluorine-19 MRI of Inflammatory Macrophage

Junsung Rho[1], **Emma Stares**[1], **Stephen R. Adams**[2], **Deanne Lister**[1], **Benjamin Leach**[1], **Eric T. Ahrens**[1,*]

[1]Department of Radiology, University of California, San Diego, La Jolla, CA 92093

[2]Department of Pharmacology, University of California, San Diego, La Jolla, CA 92093

Abstract

Purpose: We aim to develop perfluorocarbon-based nanoemulsions with improved sensitivity for detection of inflammatory macrophages *in situ* using F-19 MRI. Towards this goal, we evaluate the feasibility of nanoemulsion formulation incorporating a metal chelate in the fluorous phase which shortens the F-19 longitudinal relaxation rate and image acquisition time.

Procedures: Perfluorinated linear polymers were conjugated to metal-binding *tris*-diketonate, blended with unconjugated polymers, and emulsified in water. Phospholipid-based surfactant was used to stabilize nanoemulsion and provide biocompatibility. Nanoemulsions were metalated with the addition of ferric salt to the buffer. Physical stability of surfactant and nanoemulsion was evaluated by mass-spectrometry and dynamic light scattering measurements. Nanoemulsions were injected intravenously into a murine granuloma inflammation model, and *in vivo* ^{19}F/^{1}H MRI at 11.7 T was performed.

Results: We demonstrated stability and biocompatibility of lipid-based paramagnetic nanoemulsions. We investigated potential oxidation of lipid in the presence of metal chelate. As a proof of concept, we performed non-invasive monitoring of macrophage burden in a murine inflammation model following intravenous injection of nanoemulsion using *in vivo* F-19 MRI.

Conclusion: Lipid-based nanoemulsion probes of perfluorocarbon synthesized with iron-binding fluorinated β-diketones can be formulated for intravenous delivery and inflammation detection *in vivo*.

Keywords

MRI; fluorine-19; iron; chelate; perfluorocarbon; nanoemulsion; macrophage; inflammation; *in vivo*

*Corresponding Author: Eric T. Ahrens, University of California, San Diego, 9500 Gilman Dr. #0695, La Jolla, CA 92093-0695, Phone: (858) 246-0279, eta@ucsd.edu.

Conflict of Interest

ETA is a founder, consultant, member of the advisory board and shareholder of Celsense, Inc. The other authors declare that they have no conflicts of interest.

Introduction

Fluorine-19 (F-19) MRI is a non-invasive technique to visualize inflammation *in vivo*. Systemic administration of perfluorocarbon (PFC) nanoemulsion results in labeling of monocytes and macrophages *in situ*. Accumulation of labeled cells at inflammation sites generates tracer hot-spots which are detectable by spin-density weighted F-19 MRI with no background signal from the host's tissues due to the absence of endogenous fluorine [1]. Anatomical localization of inflammatory loci is achieved by merging the F-19 image with a conventional proton MRI scan.

Efforts to improve the F-19 MRI sensitivity include decreasing the lengthy F-19 longitudinal relaxation time (T_1) of PFC by paramagnetic relaxation enhancement (PRE) [2]. Kislukhin, et al. [3] reported formulation of a novel paramagnetic PFC nanoemulsion for F-19 imaging incorporating an iron-bound fluorinated β-diketone (FDK) chelator, i.e., ferric *tris*-diketonate (FETRIS), resulting in a shortened T_1 and potentially a multi-fold increase in imaging sensitivity. Generally, reduced T_1 enables increased signal averaging for a fixed imaging time and thus increased signal-to-noise ratio per time.

Our goal is to further develop PFC-FETRIS formulations for intravenous injection and visualization of inflammation sites *in vivo*. PFC nanoemulsions suitable for *in situ* uptake require good pharmaco-stability and biocompatibility. Thus, F-19 MRI probes for intravenous injection are often stabilized by lipids [4], such as phospholipid blends derived from egg yolk or soybean [5], which confer low toxicity and long blood circulation times of the formulation products. However, the use of lipid surfactants in conjunction with metal ions adds complexity to the formulation process, as additional concerns arise regarding the potential for oxidative damage to the lipids resulting in toxic byproducts *in vivo* [6–7].

Herein we report the formulation and characterization of the first paramagnetic fluorinated nanoemulsion for inflammation imaging. A lipid-based PFC-FETRIS formulation is described, with tunable relaxation rates and a high degree of stability *in vivo*. As a proof of concept, PFC-FETRIS for *in vivo* visualization of inflammation in a mouse model is presented.

Materials and Methods

Synthesis of FDK

Synthesis of FDK was performed as previously reported [3] with minor modifications. Briefly, 10 g of PFPE-OMe (a mixture of oligomers represented by R'O(CF$_2$CF$_2$O)$_n$CF$_2$CO$_2$Me, where R' = CF$_2$CO$_2$Me, CF$_3$ or CF$_2$CF$_3$; n = 4–16; M_n = 1750 g/mol; reactive ester groups = 1.14 mmol/gram, Exfluor Research, Round Rock, TX) was combined with *p*-methoxyacetophenone (1.25 molar equivalents relative to reactive ester group) in 20 g of dry methyl tert-butyl ether. Sodium tert-butoxide (1.25 molar equivalents relative to reactive ester group) was added and the reaction mix was stirred while immersed in a 50 °C oil bath. After two hours, heptane/acetic acid solution (80 ml of heptane + 2 ml acetic acid) was added to the mixture, forming a yellow-brown suspension which was subsequently filtered. After volatiles were removed *in vacuo*, the resulting oil was washed

with MeOH (1:1 volume to oil ratio) three times by centrifugation (3000 rpm, 1 min) and removal of the top MeOH layer. The resulting oil was further dried under high vacuum to a constant mass yielding the final product (yield 39%). The final product was confirmed with NMR (Ascend 400 MHz, Bruker Biospin, Billerica, MA). Ultra-high-resolution mass-spectrometry (MS), as described below, was used to evaluate starting material PFPE-OMe and the final product FDK.

Nanoemulsion Preparation and Characterization

For our initial *in vitro* testing, the nanoemulsion consisted of a 20–30% w/w PFC blend and L-α-phosphatidylcholine from egg yolk (EYP, 7% w/w in proportion to PFC blend, #61755, Sigma Aldrich, St. Louis, MO) in water with a total volume of 6 ml. EYP was solubilized in pure water by ultrasonication (250 W, 30% power, 9 min, Omni Ruptor, Omni International, Kennesaw, GA). The PFC blend was composed of FDK and perfluoro-15-crown-5 ether (PFCE, Exfluor Research) or perfluoropolyether (PFPE, Exfluor Research) in various proportions as needed. PFC blends were added to pre-solubilized EYP and further ultrasonicated for 2 min. The crude emulsion was passed five times through a microfluidizer (LV1, Microfluidics, Westwood, MA) operating at 20,000 psi. The final F-19 content of the resulting opalescent-white nanoemulsion was quantified by NMR using an internal standard (described below). Addition of $Fe_3(NO_3)_3$ (50 mM or 100 mM aqueous solution) was added to the nanoemulsion to yield different T_1 values, immediately resulting in a pink-red nanoemulsion. Tris base (1 M in water) was added for pH adjustment to 7.4. Propylene glycol was also added to obtain an osmolality of 290 mOsm/kg. The final nanoemulsion was filtered through 0.2 μm syringe filters (#4187, Pall Corp., Port Washington, NY) and stored at 4 °C. For *in vivo* studies, a refined formulation using highly purified lipid surfactants consisting of L-α-phosphatidylcholine (840051C, Avanti Polar Lipids, Alabaster, AL), 1,2-dipalmitoyl-*sn*-glycero-3-phosphoethanolamine (850705X, Avanti Polar Lipids), and cholesterol (700000P, Avanti Polar Lipids) in 70:2:28 molar ratio was prepared under high vacuum for removal of chloroform solvent. For simulated serum stability measurements, nanoemulsions were mixed at 10% v/v with Roswell Park Memorial Institute (RPMI) media containing 10% v/v fetal bovine serum and then kept at 37 °C. Dynamic light scattering (DLS) for size characterization was performed using a Zetasizer Nano (Malvern Instruments, Westborough, MA).

NMR

NMR spectroscopy and relaxometry measurements were obtained on a 400 MHz spectrometer. For quantitative F-19 measurements, 0.1% w/w CF_3CO_2Na in D_2O served as an internal integration reference; the F-19 NMR spectra were acquired using a single-pulse sequence with 15 s recycle time to ensure longitudinal recovery of CF_3CO_2Na. The T_1 and T_2 measurements were obtained using standard inversion recovery and Carr-Purcell-Meiboom-Gill pulse sequences, respectively, and data were analyzed using single-exponential, non-linear fitting in MestReNova software (Mestrelab, Escondido, CA).

Gas Chromatography

Chemicals—Organic solvents used in the preparation of lipid samples, as well as calibration and quality control solutions, were of the highest purity available to minimize the background level of analytes. Toluene (Optima grade), methanol (Optima LC-MS grade), dichloromethane (GC Resolv™ grade) and n-hexane (95% n-hexane; Optima grade) and hydrochloric acid (TRACESelect) were obtained from Fisher Scientific (Hamptom, NH). Ultrapure water was generated from an Advantage A10 water purification system (Millipore, Billerica, MA) fitted with LC-pak and Biopak polishers for generating LC-MS grade water free of pyrogens, bacteria and nuclease. For calibration and quality control during the quantitative analysis of fatty acid methyl esters (FAMEs), individual standards of C14, C16, C18 and C18:1 FAMEs were obtained from Sigma Aldrich and were of 99% purity.

Extraction of Lipid Fractions from Nanoemulsion Samples

Lipid fractions were extracted from nanoemulsion samples using a modified Bligh and Dyer method [8]. $CHCl_3$ (1.25 ml) and MeOH (1.25 ml) were added to a 1 ml aliquot of nanoemulsion in a 15 ml conical tube. After vortexing on high for 1 min, an additional 1.25 ml of MeOH was added, and the mixture was vortexed for 1 min. A further 1.25 ml of $CHCl_3$ was added, followed by vortexing for 1 min, and then 1.25 ml of H_2O was added, followed by vortexing for 1 min. The resulting mixture was centrifuged for 1 min at 3000 rpm. Three layers were apparent: a top layer, primarily H_2O/MeOH, a middle layer, primarily $CHCl_3$, and a small fluorous bottom layer. Orange solid was present in the fluorous layer during the process of extracting lipids from metalated nanoemulsions. The middle $CHCl_3$ layer was decanted, and the remaining mixture was extracted again with 1.25 ml of $CHCl_3$ via vortexing (1 min) and centrifugation (1 min, 3000 rpm). The combined $CHCl_3$ extracts were then washed with MeOH/H_2O (1:1, 2.5 ml) via vortexing (1 min) and centrifugation (1 min, 3000 rpm). The $CHCl_3$ extracts were then concentrated under vacuum, blanketed in N_2, and stored in darkness until analysis.

Transesterification of Lipids to FAMEs

All glassware used for the preparation and storage of samples were pre-cleaned with acetone and then combusted at 500 °C for 6 h prior to use. Lipid and nanoemulsion samples were prepared using a method adapted from Ichihara and Fukubayashi [9]. Using this method, phospholipids within the samples were hydrolyzed and esterified into their respective FAMEs, with each phospholipid molecule being converted into two FAME molecules. Prior to the transesterification procedure, the dried lipid or nanoemulsion sample was reconstituted in dichloromethane (DCM) to a final mass concentration of ~1000 mg/l (based on total mass of dried sample). Subsequently, 10 μl of the reconstituted sample (in DCM) was transferred to the bottom of a round-bottom 8 ml glass test tube, and 200 μl of toluene was added followed by 1.5 ml of methanol and then 0.3 ml of 8% HCl in 85:15 methanol:ultrapure water. The test tube mixture was vortexed and placed into an oven at 70 °C for 24 hours. The mixture was cooled to room temperature, and 1 ml of n-hexane and 1 ml of ultrapure water were added to the mixture. The n-hexane layer (containing the FAMEs) was then transferred to a 2.0 ml amber-glass autosampler vial and immediately capped and sealed using a polytetrafluoroethylene stopper.

Quantitation of FAMEs using GC-MS

The quantitation of FAMEs was performed by analyzing 1 μl aliquots of the final n-hexane extract by gas chromatography-mass spectrometry (GC-MS). GC-MS analysis was performed with a TR-5ms column (Thermo Fisher Scientific, Waltham, MA) and an oven temperature program with the following steps: 40 °C for 1 min, ramp at 10 °C/min to 320 °C, and 320 °C for 10 min. A split/splitless injector was used at 330 °C, running in pulsed splitless mode with a splitless time of 1.005 min. The carrier gas flow through the column was maintained at 1.000 ml/min. The GC-MS transfer line was maintained at 330 °C throughout the entire run. Column eluate was ionized via electron ionization with energy set at 70 eV. MS data were acquired in total ion current mode at a mass range of m/z 50–500. All quantitation of FAMEs was performed using the integrated peak areas of the extracted ion chromatogram produced by m/z 74, a common fragment ion of FAMEs during ionization in an electron ionization source. The identification of FAMEs was supported through the matching of GC-MS retention times observed in samples to those of authentic standards, as well as comparing observed TIC spectra to a MS spectral database (NIST MS Search version 2.0f, 2009).

High Resolution Mass Spectrometry

Samples were analyzed using a hybrid linear ion trap-Orbitrap mass spectrometer (Orbitrap Elite, Thermo Fisher) fitted with a heated electrospray source (HESI-LIT-Orbitrap). Samples were introduced to the HESI-LIT-Orbitrap MS by direct infusion at a flow rate of 10 μl/min. The HESI source was operated in the positive ion mode with a capillary voltage of +3.2 kV. The source temperature was maintained at 100 °C with the sheath, auxiliary, and sweep gas flows set to values of 5, 0, and 0 (arbitrary units), respectively. MS data were collected at 1 Hz for 2 min with the mass range of 100–2000 Da, and the resolution was set to 120,000 (full width at half maximum). A maximum inject time for the linear ion trap was set to 1000 ms. Following data acquisition, empirical formulas were assigned to each major peak in the MS spectra using the elemental composition calculator within the Thermo Xcalibur 4.0 software package. Calculations were performed using element ranges of 12C: 0–50, 1H: 0–100, 16O: 0–10, 14N: 0–10, 32S: 0–1, 31P: 0–1, 35Cl: 0–1 and 13C: 0–1 with a mass tolerance of 2 ppm. In addition, a limit of 10 for the double-bond equivalency was used.

In Vitro Cell Studies

In vitro cell studies were performed on a phagocytic immune cell line (RAW 264.7 cells, ATCC, Manassas, VA), cultured with RPMI containing 10% v/v fetal bovine serum, 100 μg/ml each of streptomycin and penicillin (Life Technologies, Carlsbad, CA). For toxicity assay, cells were grown to 80% confluence in a 6-well dish and incubated with cell media containing control PFC or PFC-FETRIS (5% FDK saturated with Fe^{3+}) nanoemulsion. After 4 h of labeling, cells were washed 3 times with PBS, placed in fresh media, and allowed to proliferate for 24 h in fresh media. Cells were stained with Trypan Blue to tag dead cells, and live cells were assayed using a Countess II FL Cell Counter (Life Technologies). For assessment of F-19 relaxation rate stability after *in vitro* uptake, cells were incubated with cell media containing control or PFC-FETRIS (5% or 7.5% FDK, saturated with Fe(III) at 5 mg/ml. After 4 hours, cells were washed and harvested by trypsinization. Cell pellets were

then subjected to F-19 NMR to measure $R_1 = 1/T_1$ and $R_2 = 1/T_2$ using the NMR methods described above.

In Vivo Imaging

Animal experiments were performed in accordance with the guidelines provided by the UCSD Institutional Animal Care and Use Committee (IACUC) and the National Institute of Health Guide for the Care and Use of Laboratory Animals. C57BL/6 mice (N=3, female, 6–8 weeks, Jackson Laboratory, Bar Harbor, ME) were anesthetized with 1.5% isoflurane to immobilize animals. Local inflammation was induced with a 0.3 ml injection of a 800 μg lipopolysaccharide (LPS, Sigma Aldrich) and Matrigel (Corning, Oneonta, NY) mixture subcutaneously in the posterior neck. Two hours after Matrigel implantation, a single bolus of PFCE-FETRIS (200 μl of 0.6% w/w nanoemulsion), was injected intravenously. $^1H/^{19}F$ MRI scans were performed 24 h after injection in anesthetized mice. MRI was performed using an 11.7 Tesla horizontal-bore Bruker BioSpec MRI system equipped with a double-tuned $^1H/^{19}F$ mouse volume coil and ParaVision 6 software. Images were acquired using a zero echo time (ZTE) method. The H-1 images were acquired with a repetition time (TR) of 4 ms, 1.6° flip angle, field of view 45×45×45 mm^3, and matrix size 128×128×128. F-19 images were acquired with TR = 2.4 ms, 2.6° flip angle, field of view 45×45×45 mm^3, and matrix size 64×64×64; signal averaging of recorded echoes was used to reduce impact of any residual motion, with 4 and 40 averages used for H-1 and F-19, respectively. The resulting $^{19}F/^1H$ images were imported into Fiji-ImageJ software for volume rendering and visualization. For quantitative F-19 T_1 measurements of liver *in vivo*, a saturation-recovery, point resolved spectroscopy (PRESS) sequence was used, with TE = 1.2 ms and experiments conducted with eight different TR values ranging from 49 to 6,400 ms. Following peak integration, single-exponential fits of the resulting saturation-recovery curves were performed using MestReNova software (Mestrelab, Escondido, CA).

Results

Formulation

We formulated and characterized paramagnetic fluorinated nanoemulsions for *in vivo* imaging of inflammation. Ultra-high-resolution MS of the starting material PFPE-OMe and the final product FDK was used to characterize the molecular weight distribution of each species (Fig. 1). The process for preparing lipid-stabilized FETRIS nanoemulsion is depicted in Fig. 2. The initial step involves adding the iron-binding FDK in a desired ratio to a bulk perfluorocarbon, specifically PFCE or PFPE, to form a homogenous fluorous blend [3]. The resulting perfluorocarbon blend is formulated into a colloidal suspension in aqueous buffer by the addition of lipid surfactants, followed by ultrasonication and microfluidization to yield a monodisperse nanoemulsion product.

We utilized EYP as the bulk lipid surfactant, both alone, and blended with cholesterol and the non-ionic stabilizer Cremophor [10]. Subsequently, aqueous Fe(III) is added to the pre-formed nanoemulsion, which crosses the surfactant layer to bind FDK within the fluorous phase, yielding a paramagnetic perfluorocarbon nanoemulsion [3].

Physical Properties

Physical stability of the nanoemulsions, both in storage and *in vivo*, is a key property for diagnostic applications [11]. Instability of stored nanoemulsions is mainly attributed to molecular diffusion followed by coalescence [12–13]. The PFC-FETRIS nanoemulsion displays adequate particle size stability in storage conditions at 4 °C (Fig. 3a), as measured by DLS. The stability of the formulation was also tested in serum-containing media incubated at 37 °C to simulate the *in vivo* blood plasma environment (Fig. 3b). Nanoemulsion droplet size initially increased upon incubation, presumably due to aggregation with serum proteins. However, the nanoemulsion droplet size remained stable thereafter for at least three days, which is appropriate for the timescale associated with *in situ* macrophage labeling and MRI.

The F-19 relaxation rates of PFC-FETRIS nanoemulsion can be 'tuned' by varying the FDK:PFC ratio and commensurate chelated Fe(III) concentration in the fluorous phase. For a given proportion of FDK, both relaxation rates R_1 and R_2 increase with increasing Fe(III), plateauing near at a 1:3 molar ratio of Fe(III) to FDK (Figs. 3c and 3d). This is consistent with *tris*-diketonate coordination of Fe(III) (Fig. 2) [3]. Furthermore, R_1 and R_2 exhibit a positive linear dependence on the proportion of Fe(III)-saturated FDK (Fig. 3e). Predictable relaxation rates enable consistent production of PFCE-FETRIS with relaxation times tailored to a specific imaging pulse sequence and parameter settings.

Gas Chromatography Characterization of Lipid Stability

We investigated potential lipid oxidation in the paramagnetic nanoemulsion formulations, which may result in toxic byproducts [14]. Gas chromatography was used to determine the oxidative stability of the phospholipid blend used for formulation. Following the method of Ichihara and Fukubayashi [9], lipid samples were subjected to hydrolysis and transesterification, and the resulting FAMEs were detected by GC.

Initially, a positive control sample was prepared to validate the GC method to detect changes in FAME distribution due to oxidation; a sample of EYP was deliberately oxidized by exposure to $FeSO_4$ for 24 h. As expected, the GC peaks corresponding to the unsaturated FAMEs C16:1, C18:1, C18:2 and C20:4 decreased significantly in intensity following exposure to the oxidant (Fig. 4a), thus validating GC for observing oxidation in a lipid sample.

Quantitative GC analysis was then performed on lipid fractions extracted from freshly-prepared PFC-FETRIS nanoemulsion samples formed by microfluidization. Figure 4b shows that the molar distribution of saturated and unsaturated acyl chains is preserved throughout the high-pressure emulsification process, as well as throughout the process of extracting the lipid sample.

Subsequently, we measured the change in FAME distribution of several nanoemulsion samples over four days post-emulsification. Lipid samples in triplicate were extracted from both non-metalated and metalated nanoemulsions, both stored in either air or inert nitrogen atmosphere. Figure 4c–e shows the changes in mole percent for each FAME between Day 1 and Day 4 post-formulation. No significant changes in the unsaturated fatty acids are

detected for nanoemulsions with and without Fe(III) bound in the fluorous phase, regardless of storage in air or nitrogen. All changes were within several mole percent.

In Vitro Cell Characterization and PFC-FETRIS Nanoemulsion

We performed preliminary cell toxicity studies in macrophages (RAW cells) that were labeled with PFC-FETRIS nanoemulsion *ex vivo*. Cell proliferation (Fig. 5a), 24 h post-labeling with nanoemulsion, is unchanged compared to mock-labeled cells (p = 0.46, unpaired t-test). In addition, it is important that after uptake by phagocytic cells *in vivo*, Fe(III) remains tightly bound to FDK within the fluorous phase. F-19 NMR relaxation rate measurements of labeled cell pellets were used to determine retention of Fe(III) within the emulsion droplets after exposure to the intracellular milieu. Figure 5b–c displays relaxation rates of two different % FDK concentrations of nanoemulsions before cell exposure and 24 h after uptake by RAW cells. The data show that relaxation rate enhancements, and thus iron-binding, persist post-labeling. Small (p < 0.05), increases in both R_1 and R_2 for nanoemulsion are observed (<10% in R_1 and <17% in R_2). As nanoemulsion is already iron-saturated, the origin of these small relaxation rate increases is undetermined.

In Vivo Visualization of Inflammation in Mouse

In preliminary *in vivo* experiments, we show that PFC-FETRIS can be used to detect inflammation in a mouse using F-19 MRI. We employed an established rodent inflammation model comprised of a subcutaneous injection of LPS and Matrigel [15–17] on Day 0 into the posterior neck of a C57BL/6 mouse. Intravenous injection of nanoemulsion was performed on Day 1. Representative coronal MRI data acquired on Day 4 (Fig. 6a) shows the Matrigel plug as a subcutaneous structure in the dorsal region of the ^{1}H image (Fig. 6a). The F-19 image displays hot-spots (inflammation) along the border of Matrigel plug (Fig. 6a, asterisk). F-19 is also seen in the anterior neck, presumably at lymph node (Fig. 6a). Overall, these preliminary *in vivo* data show the feasibility of using FETRIS nanoemulsion as an inflammation imaging agent.

Intravenous PFC nanoemulsion accumulates in cells of the reticuloendothelial system (RES), including monocytes/macrophages, but prominently inside Kupffer cells of the liver as seen by NMR/MRI [18]. The strong F-19 liver signal provides a reliable means to test the stability of the relaxation rate enhancement of the intracellular paramagnetic nanoemulsion over time and *in vivo*. Figure 6b shows the liver R_1 values of PFC-FETRIS, measured longitudinally in the mouse cohort using single-voxel F-19 spectroscopy; the values slowly decrease by ~30% over two weeks, possibly due to a slow loss of Fe(III) from the nanoemulsion.

Discussion

We have performed a preliminary characterization study of paramagnetic PFC nanoemulsion probes suitable for intravenous injection and macrophage imaging. This study builds on previous work by Kislukhin, et al. [3] describing the synthesis of metal-binding FDK, conjugated to linear PFC polymers, as a fluorous-soluble input, along with co-block polymers as surfactant, to formulate paramagnetic nanoemulsion imaging probes for *ex vivo*

cell labeling and '*in vivo* cytometry' [1]. The same study [3] observed that Fe(III) yielded excellent F-19 R_1 enhancement in PFC, with modest line broadening, compared to other high-spin metal ions, such as Gd^{3+} or Mn^{2+}, that are used for proton T_1 contrast agents. For future *in vivo* studies, the predictability and tunability of R_1 enhancement by varying the Fe(III) chelate concentration in the nanoemulsion enables an optimal match to scanning parameters, particularly for short repetition time (TR) acquisitions for fast imaging. Moreover, the identity and integrity of the probe *in vivo* can be monitored via *in situ* F-19 T_1 measurement.

Diamagnetic F-19 PFC probes used for intravenous injection are often stabilized by phospholipid-based surfactants to impart biocompatibility and a long plasma half-live to facilitate uptake by cells of the RES, as well as to promote agent shelf-life. Generations of PFC emulsions developed as artificial blood substitutes have employed lipid-based surfactants [19], following early toxicity concerns regarding the poloxamer-stabilized version Fluosol-DA [20–21]. Commonly, the lipid blends comprise 70–80% egg yolk phospholipid (EYP, predominantly phosphatidylcholine), along with secondary components such as cholesterol for added rigidity, or PEGylated species for improved stability and/or circulation time [6]. Egg yolk based lipids consist primarily of saturated fatty acid, which may contribute to the oxidative stability of our nanoemulsion; nanoemulsions prepared from EYP are more oxidatively stable than those prepared from soybean lecithin, which is less saturated [22].

Our results show that potential oxidative damage to lipid surfactant components is manageable for freshly prepared nanoemulsions, but this issue may be problematic for aged nanoemulsions as observed when Fe(II) salts are added in excess to the lipid-surfactant. The PFC-FETRIS nanoemulsions are formulated with Fe(III) that is less prone to oxidize lipid surfactant components such as phospholipids, although its reactivity with existing lipid hydroperoxides could result in further lipid peroxidation [23]. Furthermore, the Fe(III) is tightly bound by FETRIS and in general, chelated iron is less reactive than free iron. Oxidative damage to lipids, especially by Fe(II) involving Fenton reactions, require hydrogen peroxide (generated *in vivo* by respiration, metabolism and phagocytosis), resulting in unsaturated bond oxidation and cleavage, and generating complex lipid products that can cause subsequent biological effects [24]. Potential nanoemulsion formulation strategies to mitigate the effects of any such oxidative stress could entail the inclusion of potent scavengers of hydroxyl radical and other reactive oxygen species such as mannitol or lipid-soluble anti-oxidants such as alpha-tocoferol or astaxanthin. Use of such scavengers would require their toxicity and biocompatibility to be evaluated in formulated nanoemulsions.

Conclusion

We describe a novel paramagnetic fluorinated nanoemulsion for use in the imaging of inflammation. We have adapted PFC-FETRIS nanoemulsions for intravenous injection via the use of biocompatible lipid-based surfactants and have confirmed the physical and short-term oxidative stability of the resulting formulation. Lipid-PFC-FETRIS displays tunable

relaxometric properties and holds promise for improved F-19 MRI of inflammatory disease processes.

Acknowledgements

References

1. Ahrens ET, Zhong J (2013) In vivo MRI cell tracking using perfluorocarbon probes and fluorine-19 detection. NMR Biomed 26:860–871. [PubMed: 23606473]

2. Bloembergen N, Morgan LO (1961) Proton relaxation times in paramagnetic solutions. Effects of electron spin relaxation. J Chem Phys 34:842–850.

3. Kislukhin AA, Xu H, Adams SR, et al. (2016) Paramagnetic fluorinated nanoemulsions for sensitive cellular fluorine-19 magnetic resonance imaging. Nat Mater 15:662. [PubMed: 26974409]

4. Pelura T, Johnson C, Tarara T, Weers J (1992) Stabilization of perflubron emulsions with egg yolk phospholipid. Biomat Artif Cell Im 20:845–848.

5. Rossi M (2007) Use of lecithin and lecithin fractions In Bioactive Egg Compounds, Eds. Huopalahti R, López-Fandiño R, Anton M, Schade R. Berlin, Heidelberg: Springer Berlin Heidelberg, pp 229–239.

6. Grapentin C, Temme S, Mayenfels F, et al. (2014) Optimization of perfluorocarbon nanoemulsions for molecular imaging by ^{19}F MRI. In: Seifalian A, de Mel A, Kalaskar D, editors. Nanomedicine: One Central Press; 2014; p.268–86.

7. Minotti G, Aust S (1987) The requirement for iron (III) in the initiation of lipid peroxidation by iron (II) and hydrogen peroxide. J Biol Chem 262:1098–1104. [PubMed: 3027077]

8. Bligh EG, Dyer WJ (1959) A rapid method of total lipid extraction and purification. Can J Biochem Phys 37:911–917.

9. Ki Ichihara, Fukubayashi Y (2010) Preparation of fatty acid methyl esters for gas-liquid chromatography. J Lipid Res 51:635–640. [PubMed: 19759389]

10. Janjic J, Ahrens ET (2012) Compositions and methods for producing cellular labels for nuclear magnetic resonance techniques. United States Patent and Trade Mark Office US8227610B2.

11. Postel M, Riess JG, Weers JG (1994) Fluorocarbon emulsions - The stability issue. Artif Cell Blood Sub 22:991–1005.

12. Riess JG, Postel M (1992) Stability and stabilization of fluorocarbon emulsions destined for injection. Biomat Artif Cell Im 20:819–830.

13. Kabalnov AS, Shchukin ED (1992) Ostwald ripening theory: applications to fluorocarbon emulsion stability. Adv colloid Interfac 38:69–97.

14. Johnson DR, Decker EA (2015) The role of oxygen in lipid oxidation reactions: a review. Annual Rev Food T 6:171–190.

15. Jacoby C, Temme S, Mayenfels F, et al. (2014) Probing different perfluorocarbons for in vivo inflammation imaging by ^{19}F MRI: Image reconstruction, biological half- lives and sensitivity. NMR Biomed 27:261–271. [PubMed: 24353148]

16. Temme S, Jacoby C, Ding Z, et al. (2014) Technical advance: monitoring the trafficking of neutrophil granulocytes and monocytes during the course of tissue inflammation by noninvasive ^{19}F MRI. J Leukoc Biol 95:689–697. [PubMed: 24319285]

17. Jahromi AH, Wang C, Adams SR, et al. (2019) Fluorous-Soluble Metal Chelate for Sensitive Fluorine-19 Magnetic Resonance Imaging Nanoemulsion Probes. Acs Nano 13:143–151. [PubMed: 30525446]

18. Ahrens ET, Young W-B, Xu H, Pusateri LK (2011) Rapid quantification of inflammation in tissue samples using perfluorocarbon emulsion and fluorine-19 nuclear magnetic resonance. Biotechniques 50:229–234. [PubMed: 21548906]

19. Spahn DR (1999) Blood substitutes. Artificial oxygen carriers: perfluorocarbon emulsions. Crit Care 3:R93–97. [PubMed: 11094488]

20. Spence R, Norcross E, Costabile J, et al. (1994) Perfluorocarbons as blood substitutes: The early years: Experience with Fluosol DA-20% in the 1980s. Artif Cell Blood Sub 22:955–963.

21. Tremper KK, Vercellotti GM, Hammerschmidt DE (1984) Hemodynamic profile of adverse clinical reactions to Fluosol-DA 20%. Crit Care Med 12:428–431. [PubMed: 6713912]

22. Palacios LE, Wang T (2005) Egg-yolk lipid fractionation and lecithin characterization. J Am Oil Chem Soc 82:571–578.

23. Morrill GA, Kostellow A, Resnick LM, Gupta RK (2004) Interaction between ferric ions, phospholipid hydroperoxides, and the lipid phosphate moiety at physiological pH. Lipids 39:881–889. [PubMed: 15669764]

24. Halliwell B, Gutteridge JMC (1990) Role of free-radicals and catalytic metal-ions in man disease - an overview. Meth Enzymol 186:1–85.
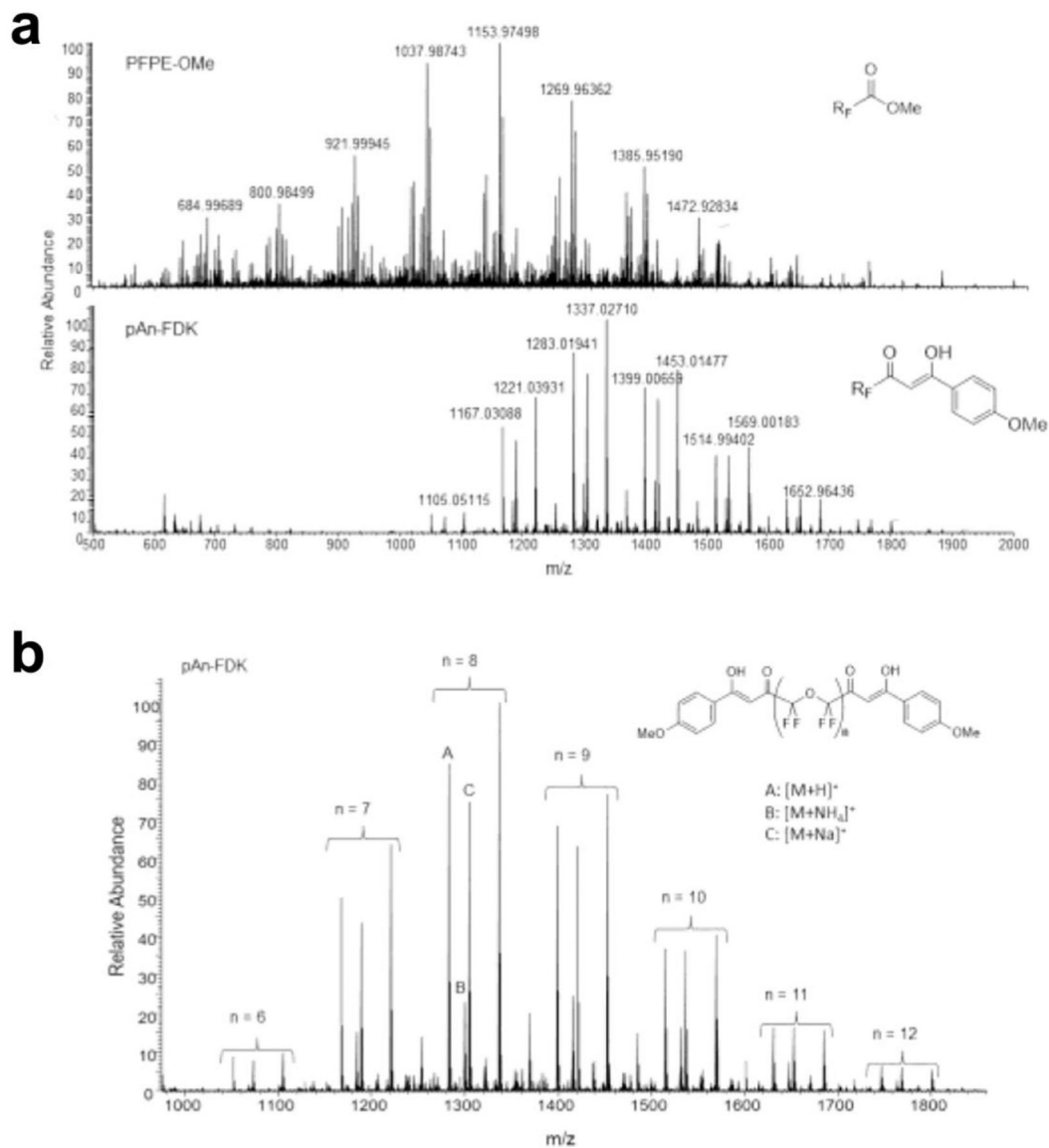
Figure 1.
Ultra-high-resolution MS data of FDK and PFPE-OMe starting materials. **a** The mass spectra of PFPE-OMe (top) and pAn-FDK (bottom) confirm complete conversion of PFPE-OMe into FDK is shown. **b** The molecular weight distribution of pAn-FDK for each species with n = 6–12 (-CF$_2$CF$_2$O-) units in the backbone.
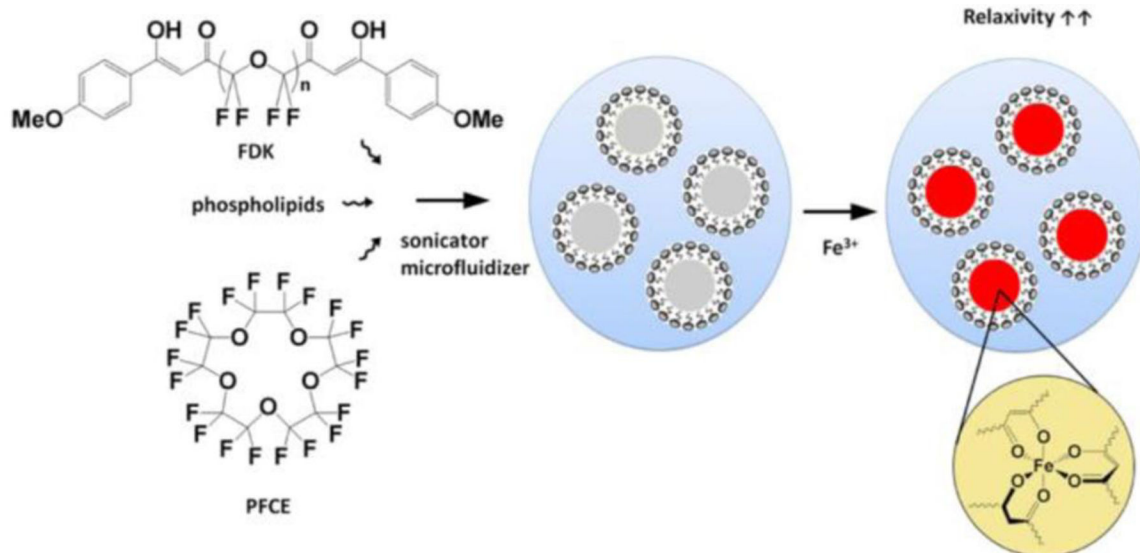
Figure 2.
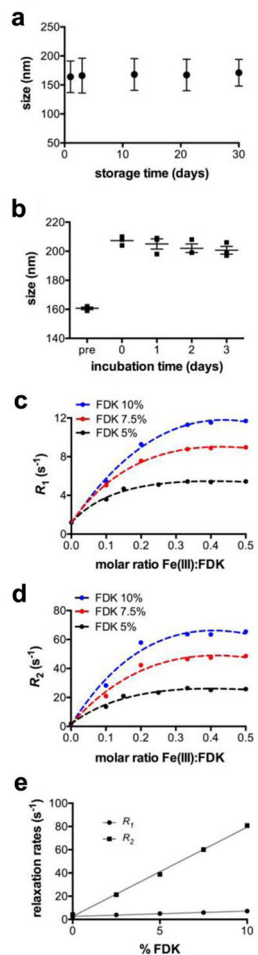Formulation of PFC-FETRIS with lipid-based surfactant.

Figure 3.

Physical properties of lipid PFCE-FETRIS nanoemulsion. **a** Droplet size measured by DLS over 30 days post-formulation. Error bars reflect the half width of polydisperity index. **b** Droplet size measured by dynamic light scattering in serum at 37 °C. "Pre" indicates measurements prior to incubation. Day 0 indicates measurements immediately after incubation. Error bars reflect standard error of the mean (N = 3). **c** Relaxation rates R_1 and **d** R_2, respectively, for lipid-FETRIS nanoemulsion formulated with bulk PFCE blended with differing amounts of FDK and Fe(III). Relaxation rates saturate at a ~1:3 molar ratio of Fe(III) to FDK. The dotted curves represent non-linear fit with R-square greater than 0.98. **e** Linear relationship between proportion of Fe(III)-saturated FDK and R_1 and R_2 for lipid-FETRIS formulated with PFPE as the bulk PFC. Lines represent linear regression with R-square greater than 0.99.
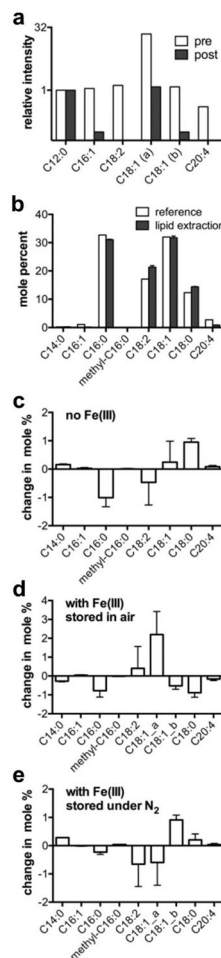
Figure 4.
Oxidation stability of lipid PFCE-FETRIS nanoemulsions. **a** The relative distribution of unsaturated FAMEs in a lipid sample pre- and post-oxidation with $FeSO_4$, normalized to the C12:0 peak. The Y-axis is in log 2 scale. **b** The FAME distribution for EYP obtained by lipid extraction from formulated nanoemulsion in comparison to reference data provided by Avanti Lipids. **c-e** The FAME distributions from day 1 to 4 post-formulation of three PFCE-FETRIS nanoemulsions are shown. The changes are expressed as differences in mole percent of total summed FAMEs. C18:1_a and C18:1_b denote are cis and trans isomers, respectively. Error bars represent standard deviations calculated from three separately hydrolyzed lipid samples.
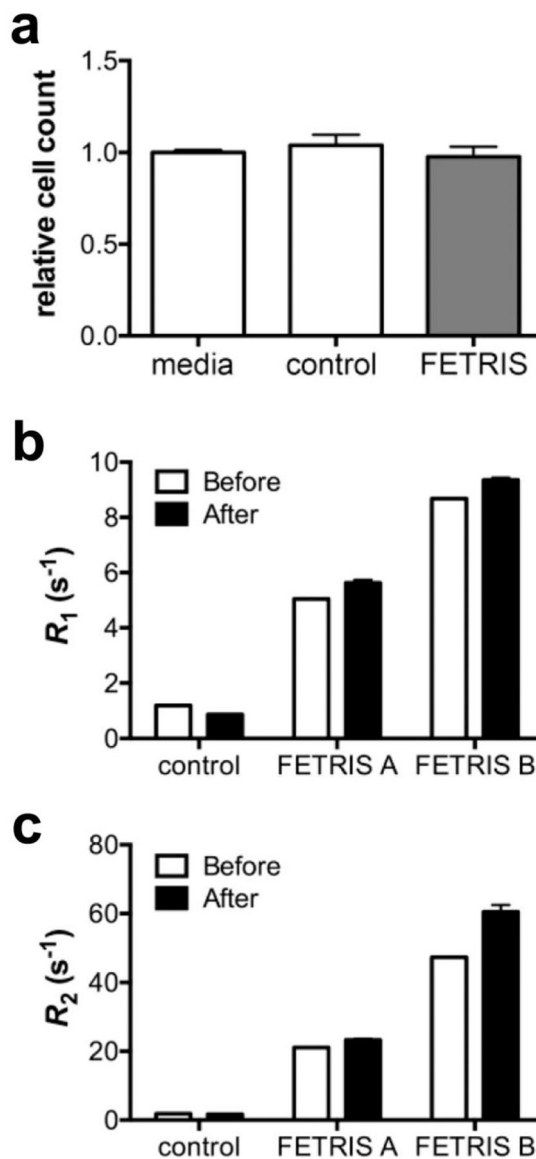
Figure 5.
In vitro cell characterization of lipid PFCE-FETRIS nanoemulsion labeled cells. **a** Unhindered proliferation via cell counts in RAW cells post-exposure to lipid-PFCE-FETRIS nanoemulsion, where cell counts are normalized to the media-treated control. Control nanoemulsion consists of PFCE without FDK or Fe(III). Unpaired t-test indicates no significant difference between groups, $p = 0.46$. **b** R_1 and **c** R_2 relaxation rates show persistent relaxation enhancement in PFCE-FETRIS nanoemulsion-labeled RAW cells (After) as referenced to FETRIS-free nanoemulsion (Before). Two formulations of lipid-PFCE-FETRIS nanoemulsion were tested, *i.e.*, 5 (FETRIS A) and 7.5 (FETRIS B) % FDK, both Fe(III) saturated. Error bars are standard deviation of the mean ($N = 3$).
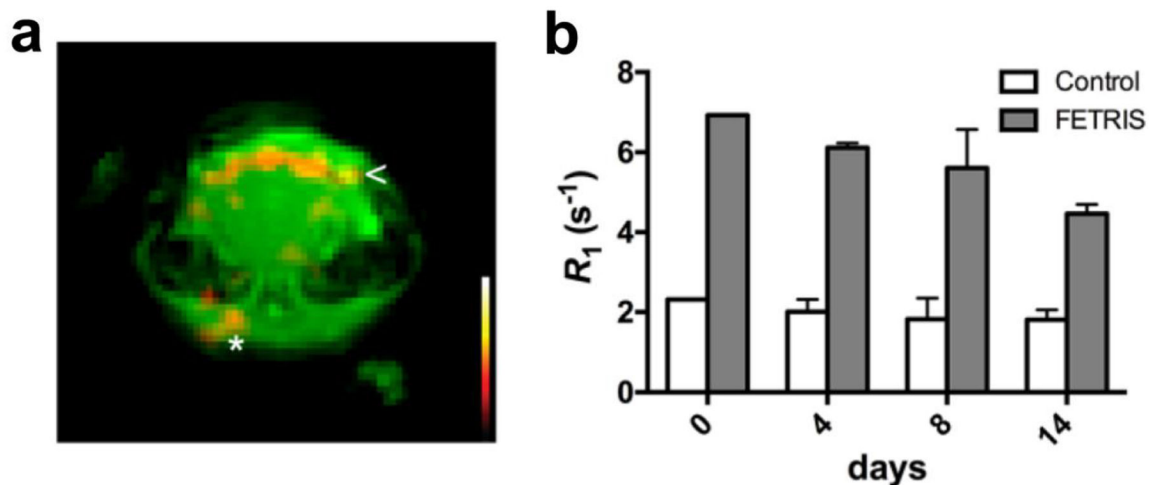
Figure 6.

In vivo ^{19}F/^{1}H MRI study in murine inflammation model. Localized acute inflammation was induced by subcutaneous injection of LPS-Matrigel in dorsal head region. One day after intravenous injection of PFC-FETRIS, ^{1}H/^{19}F MRI data in the plug region were acquired at 11.7 T using a ZTE pulse sequence. **a** The ^{1}H coronal image (green) shows the brain and Matrigel plug in the subcutaneous tissue on dorsal head. The hot-iron color scale (inset) F-19 image displays apparent macrophage infiltrates in inferior Matrigel plug (arrow) and nearby lymph node (asterisk). **b** The longitudinal stability of R_1 *in vivo* measured using localized F-19 spectroscopy of the liver over 14 days post-injection. Error bars are standard deviation of the mean (N = 3).